Ocean Salinities Reveal Strong Global Water Cycle Intensification during 1950-2000*

Paul J. Durack[1,2,3,4]✚, Susan E. Wijffels[1,3] and Richard J. Matear[1,3]

[1]*Centre for Australian Weather and Climate Research, Commonwealth Scientific and Industrial Research Organisation (CSIRO) Marine and Atmospheric Research, General Post Office (GPO) Box 1538, Hobart, Tasmania 7001, Australia*

[2]*Institute for Marine and Antarctic Studies, University of Tasmania, Private Bag 129, Hobart, Tasmania 7001, Australia*

[3]*Wealth from Oceans National Research Flagship, CSIRO, GPO Box 1538, Hobart, Tasmania 7001, Australia*

[4]*Program for Climate Model Diagnosis and Intercomparison, Lawrence Livermore National Laboratory, Mail Code L-103, 7000 East Avenue, Livermore, CA 94550, USA*

✚ *To whom correspondence should be addressed. E-mail: pauldurack@llnl.gov*

DOI: 10.1126/science.1212222

Under embargo with Science Magazine – not for release until 2:00 pm U.S. Eastern Time Thursday, 26 April 2012

Summary sentence: New estimates of water cycle intensification inferred from observed ocean salinity changes suggest a 4% intensification has occurred from 1950 to 2000, twice the response projected by current generation global climate models.

Abstract: Fundamental thermodynamics and climate models suggest that dry regions will become drier and wet regions will become wetter in response to warming. Efforts to detect this long-term response in sparse surface observations of rainfall and evaporation remain ambiguous. We show that ocean salinity patterns express an identifiable fingerprint of an intensifying water cycle. Our 50 year observed global surface salinity changes, combined with changes from global climate models, present robust evidence of an intensified global water cycle at a rate of 8% ± 5% per degree of surface warming. This rate is double the response projected by current generation climate models and suggests that a substantial (16 to 24%) intensification of the global water cycle will occur in a future 2° to 3° warmer world.

Introductory paragraph: A warming of the global surface and lower atmosphere is expected to strengthen the water cycle (*1-3*) largely driven by the ability of warmer air to hold and to redistribute more moisture. This intensification is expressed as an enhancement in the patterns of surface water fluxes [evaporation and precipitation (E-P)] and, as a consequence, ocean surface salinity patterns. According to the Clausius-Clapeyron (CC) relation and assuming a fixed relative humidity, we expect a ~7% increase in atmospheric moisture content for every degree of warming of Earth's lower troposphere (*2*). Of greatest importance to society, and the focus of this work, is the strength of the regional pattern of (E-P), which in climate models scales approximately with CC, whereas global precipitation changes more slowly at a rate of 2 to 3% $°C^{-1}$, limited by tropospheric energy constraints (*2, 4*).

An intensification of existing patterns of global mean surface (E-P) is found along with enhancements to extreme events such as droughts and floods (*1, 5*) in available 21st century climate projections, forced by anthropogenic greenhouse gases (GHGs) from the Coupled Model Intercomparison Project Phase 3 [CMIP3 (*6*)]. This has been labelled the "rich get richer" mechanism, where wet areas (compared with the global mean) get wetter and dry regions drier (*7*). There is, however, little consistency in the seasonal changes provided by model projections and poor agreement when compared with regional observational estimates (*8*). Additionally, atmospheric aerosols included in these projections can regionally counteract the GHG-driven warming and act to suppress the local water cycle through dynamical changes (*9, 10*).

Given the above broad-scale model responses and the CC relationship, an intensification of ~4% in the global water cycle (E-P) is expected to already have occurred in response to the observed 0.5°C warming of Earth's surface over the past 50 years (*11*). However, obtaining a global view of historical long-term rainfall pattern changes is made difficult because of the spatially sparse and short observational record. Long, high-quality land-based records are few and Northern Hemisphere biased (*12*). Direct high quality long-term rainfall estimates over oceans [which comprise 71% of the global surface area and receive over 80% of global rainfall (*13*) (Fig. S1)]

are very scarce, with most global observational products dependent on data contributions from satellites, themselves sensitive to error (*14, 15*). Additionally, because of the short temporal coverage (~15 to 30 years) by satellite missions, trends are likely affected by natural decadal modes of variability and may dominate much of the measured changes (*3*). This challenge is exacerbated by the spatially and temporally sporadic nature of rainfall, making the derivation of broad-scale averages of small multidecadal changes from a sparse network of observing stations error-prone (*16*). These difficulties are evident in the differing signs of long-term trends between reconstructed rainfall datasets (*17, 18*). Discrepancies among air-sea evaporative flux products (*19*) undermine their use in resolving long-term water cycle changes. As a result, we do not yet have a definitive view on whether Earth's water cycle has intensified over the past several decades from atmospheric observing networks (*12, 20*).

It has long been noted that the climatological mean sea surface salinity (SSS) spatial pattern is highly correlated with the long-term mean E-P spatial pattern (*21*) (Fig. 1, A and D), reflecting the balance between ocean advection and mixing processes and E-P forcing at the ocean surface (*21-23*). Several studies of multidecadal SSS changes reveal a clear pattern where increasing salinities are found in the evaporation dominated mid-latitudes and decreasing salinities in the rainfall dominated regions such as the tropical atmospheric convergence zones and polar regions (*22, 24-28*). These previous studies have used optimally averaged pentadal historical ocean data (*24*) or the difference between pre-2000 and post-2000 climatologies (*27*), the latter period being strongly supported by the modern baseline provided by the Argo Programme (*29*) to investigate long-term salinity changes in the global ocean. By using a direct local fit of trends to historical and Argo data simultaneously (*25*), we map the multidecadal linear SSS trends back to 1950 (Fig. 1, D and G). Over the last 50 years SSS changes reflect an intensification of the mean SSS patterns. This strong and coherent relationship is expressed through the high spatial pattern correlation coefficient (PC) of ~0.7 (Fig. S2) between the mean SSS and independent estimates of long-term SSS change. Following the "rich get richer"

mechanism (*7*), salty ocean regions (compared to the global mean) are getting saltier, whereas fresh regions are getting fresher (*24-28*). This robust intensification of the observed SSS pattern is qualitatively consistent with increased E-P if ocean mixing and circulation are largely unchanged.

In trying to quantitatively relate SSS changes and E-P changes previous studies have made strong simplifying assumptions. One estimate of a global 3.7% E-P intensification from 1970s to 2005 (*27*) is based on the assumption of an unchanging ocean mixing and advection field, with the additional assumption that no salt or freshwater exchange has occurred over this time with the ocean below 100m. However, several studies have shown subsurface salinity changes have occurred during the 20th century (*24, 25*), with many of the largest signals expressed at depths greater than 100m. Another study used subsurface salinity changes on isopycnals to deduce E-P changes at the surface density outcrops (*26*). This approach is error prone because broad-scale salinity changes on density surfaces can largely be explained by the subduction of broad-scale warming and not E-P changes alone (*25*). To avoid such strong assumptions and explore the use of SSS pattern changes as a water cycle diagnostic, we used the most comprehensive simulations available to date of the historical and future global climate: the CMIP3 simulations of the 20th century (20C3M) and the Special Report on Emissions Scenarios (SRES) 21st century future projections (*6*). Within these simulations we investigated the relationship between SSS and E-P pattern changes. These simulations capture the full range of complex dynamical changes in response to GHG forcing, which include ocean surface (and subsurface) temperature changes, dynamical shifts to ocean and atmospheric circulation, upper ocean stratification changes as well as the regional effects of aerosols on water cycle operation.

To quantify and compare the strength of broad-scale SSS pattern intensification in both observations and CMIP3, we formed zonal ocean basin (Pacific, Atlantic and Indian) averages for both the 50 year (1950-2000) climatological mean SSS and its 50 year (1950-2000) linear trends. A linear regression was undertaken by using the basin zonal averages of the

climatological mean SSS (*x* axis) anomaly from the global climatological SSS against the SSS change pattern (*y* axis; Fig. 1, J). We defined the resulting slope of this relationship as the pattern amplification (PA) and the corresponding correlation coefficient (R) as the pattern correlation (PC). A key advantage of this analysis is its insensitivity to the mean spatial climatological biases in model fields (*30*) when compared to observations, because the model change fields are compared to their own model climatology. We formed the PA and PC metrics for each model simulation and our observational analysis (Fig. S2 presents comparative basin zonal mean analyses for available global SSS studies; see supplementary text section 1.1).

Analysis of trends in observed SSS indicates that from 1950 to 2000 the SSS PA is 8% with a PC of 0.7 (Fig. 1J). Similar to observations, many models show a high PC (~0.7 to 0.9) between the climatological mean SSS and the corresponding climatological mean E-P. However, most 20C3M model simulations show a weaker than observed spatial PC and PA between the 50 year SSS mean and SSS change patterns (Fig. 1, D and G versus E and H, F and I) and do not uniformly provide a realistic simulation of observed surface mean SSS patterns or its change over 1950-2000 (Fig. 1, D and G; Fig. S6; Table S2; and supplementary text section 2). Our examples of the simulations that most closely replicate the observed spatial change and mean patterns (Fig. 1, E and H) and those that produce an almost inverse spatial change pattern (Fig. 1, F and I) compared with the observed results (Fig. 1, D and G) illustrate the range of responses found in CMIP3 (Fig. 1). Some models show similar numbers to those observed (Fig. 1, E, H and K), whereas others have very low values of both PA and PC (Fig. 1, F, I and L), indicating no clear SSS pattern amplification. Such discrepancies raise a key question: What controls this difference in the modelled SSS response and how is this related to water cycle changes?

The PA and PC methodology can also be used when considering other variables, such as the surface water flux (E-P). CMIP3 simulations show a relationship between SSS PA and the E-P PA (Fig. 2B). This key result supports the use of SSS PA as a diagnostic of a changing water cycle and also provides a relationship in which to consider the observed SSS PA for 1950-2000. The

CMIP3 SSS patterns amplify at twice the rate of E-P patterns (Fig. 2B). The reason that E-P PA drives a stronger response in SSS PA for CMIP3 is not clearly understood and requires further investigation, but the relationship between them is compelling.

When investigating water cycle changes, it is important to consider the coincident global surface warming, the natural thermodynamic framework of water cycle amplification. If expressed in a per degree warming context, such water cycle rate changes can then be directly compared to other studies, both oceanographic and atmospheric in their origins (Table S3; Fig. S9; and see supplementary text section 4).

For both the 20C3M and SRES CMIP3 simulations, we find a relationship between the rate of global average surface warming (ΔTa) and the rate of SSS PA and PC strength (Fig. 2A). The 20C3M simulations in which the warming rate is low (generally those with comprehensive aerosol schemes; contrast diamonds and circles in Fig. S5; Table S1; and see supplementary text section 2.2) feature low SSS PA, with spatial change patterns having only slight correspondence to the spatial mean pattern and consequently a low SSS PC (illustrated by the simulation in Fig. 1, F, I and L). The stronger warming SRES simulations express a clearer and larger pattern amplification response (PC > 0.5) than most 20C3M simulations (Fig. 2A). The increase in PC with enhanced PA suggests a signal-to-noise process is operating, whereas in weakly warming simulations model internal variability dominates the change signal. A PC-weighted line of best fit through the 93 CMIP3 simulations suggests that SSS patterns intensify with warming at 8% $°C^{-1}$ (Fig. 2A), which is half of our 1950-2000 observed rate (16% $°C^{-1}$; Fig. 2A). As expected on the basis of past analyses of CMIP3 (*2*), the E-P PA is also linearly related to surface warming rates (Fig. 2C) with the model line of best fit below CC (4.5% $°C^{-1}$). Also in agreement with many previous analyses (*1, 2*), total global average rainfall is linearly related to warming rates but with a distinctively weaker slope than surface water flux, near 3.1% $°C^{-1}$ (Fig. 2D). The stronger SSS PA response to warming and the tighter agreement among CMIP3 when compared with that for the E-P PA (Fig. 2, A versus C) suggest that long-term SSS pattern changes provide an

identifiable, highly detectable and particularly sensitive measure of long-term water cycle changes. It is likely that ocean mixing and circulation act to integrate and smooth the temporal and spatial patchiness of E-P fluxes at the ocean surface and provide a smoothed SSS anomaly field, which facilitates detection of broad-scale, persistent changes.

To independently demonstrate the strong relationship between 50 year salinity change and an enhanced water cycle, we explored the response of an ocean-only model to an idealized 5% E-P pattern increase. We used a version of the MOM3 ocean model, forced with E-P fields obtained from the National Centers for Environmental Prediction (NCEP) reanalysis. A linear trend in E-P was imposed to achieve a 5% increase over 50 years. The resulting spatial pattern of SSS change strongly mirrors the observed and CMIP3 ensemble mean patterns but with smaller absolute magnitudes (Fig. 3, A, C and D versus B). The salinity pattern amplification is expressed for surface and subsurface changes (Figs. S7 and S8; and supplementary text section 3). Therefore in a global ocean-only model, spatial salinity patterns enhance in response to an intensified E-P. A similar spatial response to the observed changes are found in CMIP3 but only for the strongly warming 20C3M simulations (>0.5°C; Fig. 3, D versus C). Those simulations with less than the observed warming over 1950-2000 often incorporate aerosol effects that act to reduce warming (contrast diamonds and circles in Fig. S5) and thus under predict the subsequent water cycle amplification as expressed in SSS changes.

Despite their scatter, estimates from the CMIP3 ensemble show a weaker salinity pattern amplification per degree of warming (8% $°C^{-1}$; Fig. 2A) than has been observed (16% $°C^{-1}$; Fig. 2A). By using the modelled relationship between SSS PA and E-P PA from the CMIP3 ensemble [which shows that SSS PA increases at twice the rate of E-P PA (Fig. 2B)] and applying this relationship to our observed SSS PA estimate, we infer that over the past 50 years the global water cycle has amplified by 4%. Using the observed 0.5°C surface warming estimate (*11*), this inferred water flux amplification of 8% $°C^{-1}$ is close to that predicted by the CC relationship (~7% $°C^{-1}$). This rate of change is consistent with many other independent observational estimates

(Table S3 and Fig. S9) which all provide evidence that an observed global water cycle amplification has occurred. However, CMIP3 ensemble averages of E-P PA produce a rate well below this of 4.5% $°C^{-1}$ (Fig. 2C).

A change to freshwater availability in response to climate change poses a more important risk to human societies and ecosystems than warming alone. Changes to the global water cycle and the corresponding redistribution of rainfall will affect food availability, stability, access and utilisation. We show that ocean salinity is a particularly sensitive marker of water cycle change that provides us with a salty ocean-freshwater "gauge" from which to monitor 71% of Earth's surface. By using ocean observations we show the "rich get richer" mechanism is already operating, with fresh regions becoming fresher and salty regions saltier in response to observed warming. Our results support a water cycle intensification rate consistent with the CC relationship under fixed relative humidity. In a future GHG-forced 2° to 3°C warmer world (*31*), this implies a 16 to 24% amplification of the global water cycle will occur, nearly double the CMIP3 response.

Acknowledgments This work has been undertaken as part of the Australian Climate Change Science Program, funded jointly by the Department of Climate Change and Energy Efficiency, the Bureau of Meteorology and CSIRO. P.J.D. was supported by a joint QMS-University of Tasmania Ph.D. scholarship in Quantitative Marine Science (QMS) with support from CSIRO's Wealth from Oceans Flagship. Work undertaken at Lawrence Livermore National Laboratory is supported by the U.S. Department of Energy under contract DE-AC52-07NA27344. We acknowledge the modeling groups, the Program for Climate Model Diagnosis and Intercomparison (PCMDI) and the WCRP's Working Group on Coupled Modelling (WGCM) for their roles in making available the WCRP CMIP3 multi model data set. We thank numerous colleagues from CSIRO, the Centre for Australian Weather and Climate Research (CAWCR), and the University of Tasmania for valuable feedback and input into this project. The Centre for Australian Weather and Climate Research is a partnership between CSIRO and the Australian Bureau of Meteorology. We also thank J. Durack of the University of California at Berkeley, S. Griffies of the Geophysical Fluid Dynamics Laboratory (GFDL), and R. Colman of CAWCR for helpful comments with early drafts of this manuscript. We acknowledge the reviewers: J. Fasullo of the National Center for Atmospheric Research, R. Schmitt of Woods Hole Oceanographic Institution and an anonymous third reviewer for their feedback which strongly improved the manuscript. Observed salinity change data can be downloaded from the CSIRO Ocean Change Web site at http://www.cmar.csiro.au/oceanchange.

Author Contributions P.J.D. conceived the study, completed the analysis, and shared responsibility for writing the manuscript. S.E.W. assisted in the analysis and shared responsibility for writing the manuscript. R.J.M. undertook the idealized model simulations. All authors contributed to the final version of the manuscript.

References and Notes

1. M. R. Allen, W. J. Ingram, Constraints on future changes in climate and the hydrologic cycle. Nature 419, 224 (2002).
2. I. M. Held, B. J. Soden, Robust Responses of the Hydrological Cycle to Global Warming. Journal of Climate 19, 5686 (2006).
3. F. J. Wentz, L. Ricciardulli, K. Hilburn, C. Mears, How Much More Rain Will Global Warming Bring? Science 317, 233 (July 13, 2007, 2007).
4. G. L. Stephens, Y. Hu, Are climate-related changes to the character of global-mean precipitation predictable? Environmental Research Letters 5, 025209 (2010).
5. S. Emori, S. J. Brown, Dynamic and thermodynamic changes in mean and extreme precipitation under changed climate. Geophys Res Lett 32, L17706 (2005).
6. G. A. Meehl et al., The WCRP CMIP3 multimodel dataset - A new era in climate change research. B Am Meteorol Soc 88, 1383 (Sep, 2007).
7. C. Chou, J. D. Neelin, C.-A. Chen, J.-Y. Tu, Evaluating the "Rich-Get-Richer" Mechanism in Tropical Precipitation Change under Global Warming. Journal of Climate 22, 1982 (2009/04/01, 2009).
8. G. L. Stephens et al., Dreary state of precipitation in global models. Journal of Geophysical Research 115, D24211 (2010).
9. V. Ramanathan, P. J. Crutzen, J. T. Kiehl, D. Rosenfeld, Aerosols, Climate, and the Hydrological Cycle. Science 294, 2119 (December 7, 2001, 2001).
10. Y. Ming, V. Ramaswamy, G. Persad, Two opposing effects of absorbing aerosols on global-mean precipitation. Geophys Res Lett 37, L13701 (2010).
11. K. E. Trenberth et al., in Climate Change 2007: The Physical Science Basis. Contribution of the Working Group I to the Fourth Assessment Report of the Intergovernmental Panel on Climate Change, S. Solomon et al., Eds. (Cambridge University Press, Cambridge UK and New York USA, 2007), pp. 235-336.
12. X. Zhang et al., Detection of human influence on twentieth-century precipitation trends. Nature 448, 461 (2007).
13. J. J. Schanze, R. W. Schmitt, L. L. Yu, The global oceanic freshwater cycle: A state-of-the-art quantification. Journal of Marine Research 68, 569 (2010).
14. Y. Tian et al., Component analysis of errors in satellite-based precipitation estimates. Journal of Geophysical Research 114, D24101 (2009).
15. X. Yin, A. Gruber, P. Arkin, Comparison of the GPCP and CMAP Merged Gauge–Satellite Monthly Precipitation Products for the Period 1979–2001. Journal of Hydrometeorology 5, 1207 (2004).
16. A. Dai, I. Y. Fung, A. D. Del Genio, Surface Observed Global Land Precipitation Variations during 1900–88. Journal of Climate 10, 2943 (1997).
17. P. A. Arkin, T. M. Smith, M. R. P. Sapiano, J. Janowiak, The observed sensitivity of the global hydrological cycle to changes in surface temperature. Environmental Research Letters 5, 035201 (2010).
18. K. M. Lau, H. T. Wu, Detecting trends in tropical rainfall characteristics, 1979–2003. International Journal of Climatology 27, 979 (2007).
19. J. Liu, T. Xiao, L. Chen, Intercomparisons of Air–Sea Heat Fluxes over the Southern Ocean. Journal of Climate 24, 1198 (2011).
20. A. Dai, T. Qian, K. E. Trenberth, J. D. Milliman, Changes in Continental Freshwater Discharge from 1948 to 2004. Journal of Climate 22, 2773 (2009).
21. G. Wüst, in Länderkundliche Forschung. (Festschrift Norbert Krebs, Stuttgart, Germany, 1936), pp. 347-359.
22. P. J. Durack, S. E. Wijffels, N. L. Bindoff, Ocean Salinity: A Water Cycle Diagnostic? . B Am Meteorol Soc 92, s91 (2011).
23. R. W. Schmitt, Salinity and the Global Water Cycle. Oceanography 21, 14 (Mar, 2008).
24. T. P. Boyer, S. Levitus, J. I. Antonov, R. A. Locarnini, H. E. Garcia, Linear trends in salinity for the World Ocean, 1955-1998. Geophys Res Lett 32, L01604 (2005).

25. P. J. Durack, S. E. Wijffels, Fifty-Year Trends in Global Ocean Salinities and Their Relationship to Broad-Scale Warming. Journal of Climate 23, 4342 (2010).
26. K. P. Helm, N. L. Bindoff, J. A. Church, Changes in the global hydrological-cycle inferred from ocean salinity. Geophys Res Lett 37, L18701 (2010).
27. S. Hosoda, T. Sugo, N. Shikama, K. Mizuno, Global Surface Layer Salinity Change Detected by Argo and Its Implication for Hydrological Cycle Intensification. Journal of Oceanography 65, 579 (2009).
28. N. L. Bindoff et al., in Climate Change 2007: The Physical Science Basis. Contribution of the Working Group I to the Fourth Assessment Report of the Intergovernmental Panel on Climate Change, S. Solomon et al., Eds. (Cambridge University Press, Cambridge UK and New York USA, 2007), pp. 385-432.
29. H. Freeland et al., in Proceedings of OceanObs'09: Sustained Ocean Observations and Information for Society, J. Hall, D. E. Harrison, D. Stammer, Eds. (Venice, Italy, 2010), vol. 2.
30. J.-L. Lin, The Double-ITCZ Problem in IPCC AR4 Coupled GCMs: Ocean–Atmosphere Feedback Analysis. Journal of Climate 20, 4497 (2007).
31. G. A. Meehl et al., in Climate Change 2007: The Physical Science Basis. Contribution of the Working Group I to the Fourth Assessment Report of the Intergovernmental Panel on Climate Change, S. Solomon et al., Eds. (Cambridge University Press, Cambridge UK and New York USA, 2007), pp. 747-845.
32. S. A. Josey, E. C. Kent, P. K. Taylor, "The Southampton Oceanography Centre (SOC) Ocean - Atmosphere, Heat, Momentum and Freshwater Flux Atlas" (Southampton Oceanography Centre, Southampton, UK, 1998).

Figures

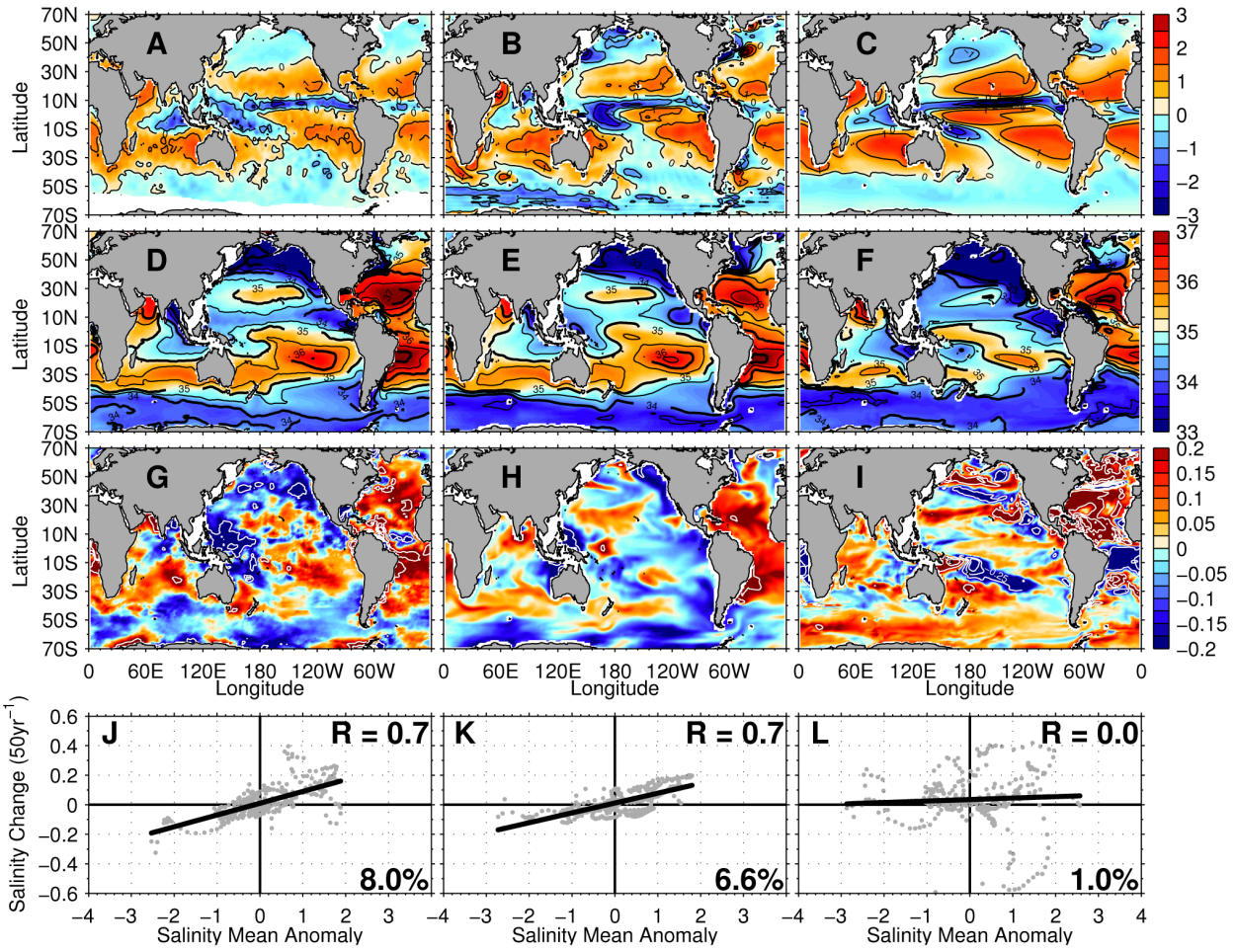

Figure 1. Observed and selected CMIP3 20C3M simulations of surface salinity and water fluxes. Surface annual mean water flux from 1950 to 2000 (E-P m year^{-1})(A to C). Surface annual mean salinity 1950-2000 (PSS-78)(D to F). Surface salinity change 1950-2000 (PSS-78 50 year^{-1})(G to I). Basin zonal-mean surface salinity trends (*y* axis) versus basin surface mean salinity anomaly from the surface basin zonal mean; in text these are the PA (slope) and PC (correlation coefficient, *R*)(J to L). The observed result of (25) [(D), (G), and (J)] and (A) the observed result of (32) for 1980-1993. Results from the Canadian Centre for Climate Modelling and Analysis, CGCM3.1 (T63) model [(B), (E), (H), and (K)] and results from the United Kingdom MetOffice, HadGEM1 model [(C), (F), (I), and (L)]. For (A) to (C), black contours mark every 1 m year^{-1}. For (D) to (F), black contours represent surface mean salinity every 1 PSS-78 for bold lines and 0.5 for thin. For (G) to (I), white contours represent surface salinity change every 0.25 PSS-78.

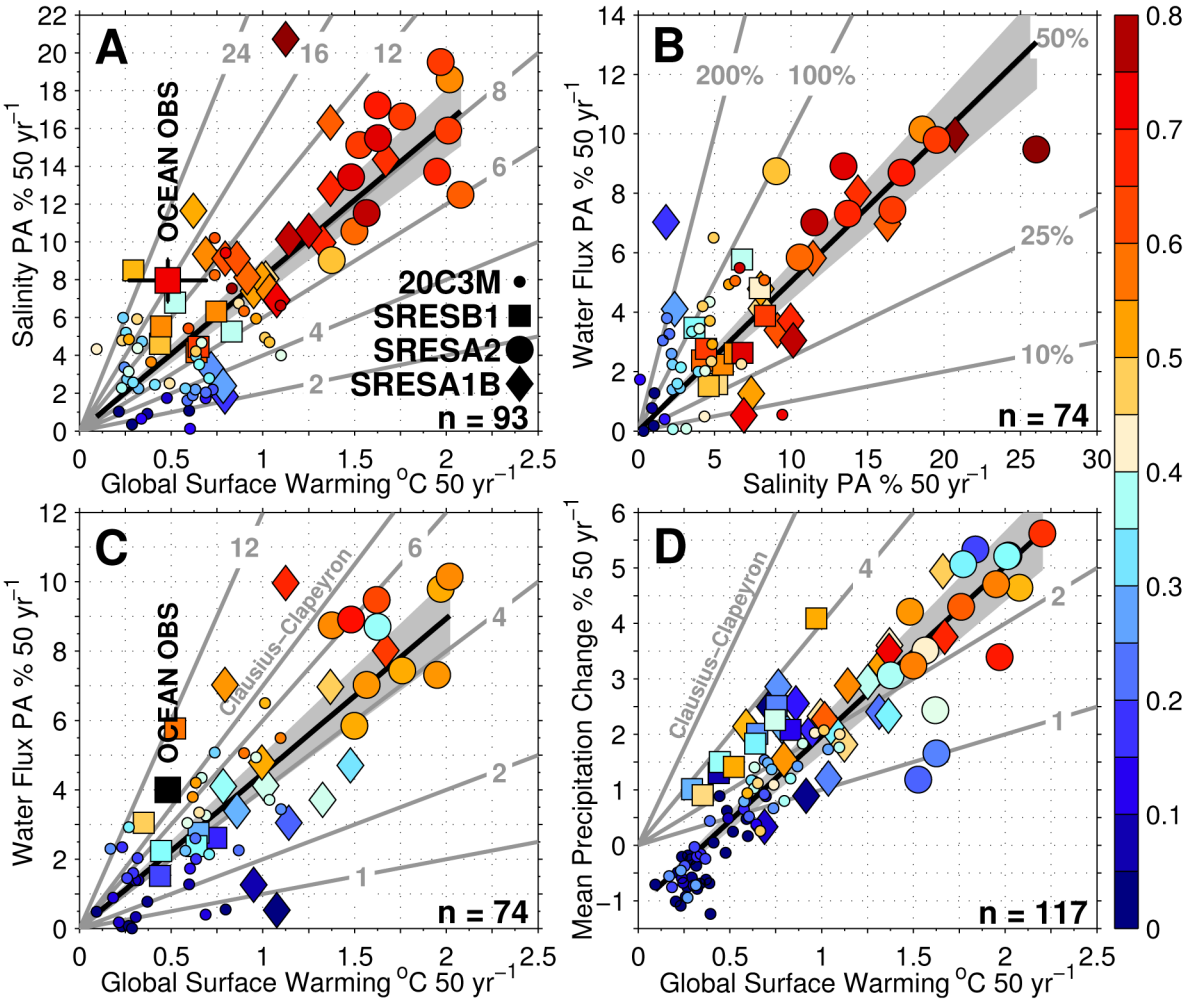

Figure 2. Pattern amplification (PA) and pattern correlation (PC) values from the available CMIP3 simulations compared with new observational estimates. The number of individual simulations that have been analysed for each variable is noted in the bottom right hand corner of each panel. (A) The surface salinity PA (*y* axis) versus the corresponding global average surface temperature change (Δ*Ta*) (*x* axis), colors are the salinity PC. (B) Water flux (E-P; *y* axis) PA versus surface salinity PA (*x* axis), colors are the salinity PC. (C) Water flux (E-P; *y* axis) PA versus global Δ*Ta* (*x* axis), colors are the E-P PC. (D) Global spatial average precipitation change, rather than PA (ΔP; *y* axis) versus global Δ*Ta* (*x* axis), colors are the precipitation PC. Gray lines express constant proportional change. Gray shading [99% confidence interval (C.I.)] bounds the PC-weighted linear best fit to the model ensemble for a line intersecting 0 [*y* axis in (A) to (C)] and -1.1 [*y* axis in (D)] in black. The 20th century (20C3M; 1950-2000) simulations are presented in small circles, and the three 21st century projected scenarios (SRES; 2050-2099) are shown as squares for B1, large circles for A2, and diamonds for A1B. All simulations have been de-drifted by using an appropriate pre industrial control simulation for the period 1900-2049 (see supplementary text section 2). Observational estimates using a Δ*Ta* value from HadCRUT3 in (A) PA from this study are shown as the red square with black error bars showing the 99% significance level and in (C) as the black square with the CMIP3-scaled result based from (A)(see text).

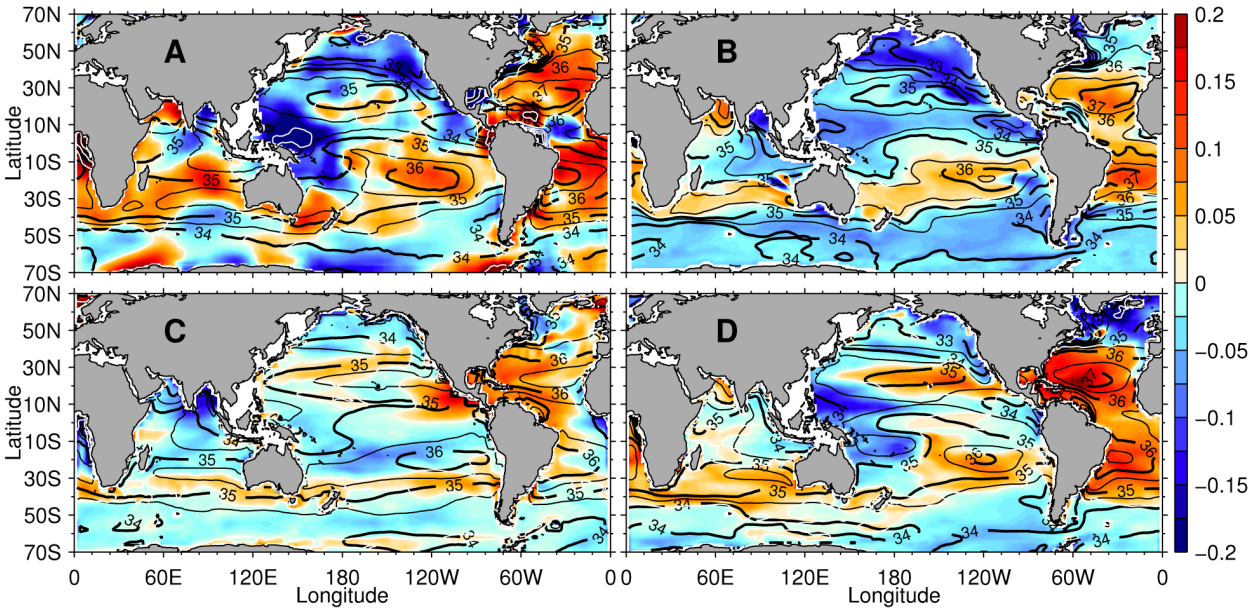

Figure 3. Patterns of 50 year surface salinity change (PSS-78 50 year^{-1}). (A) The 1950-2000 observational result of (25). (B) From an ocean model forced with an idealized surface 5% E-P enhancement (50 year^{-1}; see text). (C) For an ensemble mean from 1950-2000 of the CMIP3 20C3M simulations that warm <0.5°C (24 simulations; see Table S2). (D) For an ensemble mean from 1950-2000 of the CMIP3 20C3M simulations that warm >0.5°C (26 simulations; see Table S2). In each panel, the corresponding mean salinity from each representative data source is contoured in black, with thick lines every 1 (PSS-78) and thin lines every 0.5 (PSS-78).